Journal of Catalysis 281 (2011) 290–299

Contents lists available at ScienceDirect

Journal of Catalysis

journal homepage: www.elsevier.com/locate/jcat

Interconversion between γ-valerolactone and pentenoic acid combined with decarboxylation to form butene over silica/alumina

Jesse Q. Bond, Dong Wang, David Martin Alonso, James A. Dumesic *

Department of Chemical and Biological Engineering, University of Wisconsin, Madison, WI 53706, USA

ARTICLE INFO

Article history:
Received 20 October 2010
Revised 6 May 2011
Accepted 10 May 2011
Available online 15 June 2011

Keywords:
γ-Valerolactone
Pentenoic acid
Butene
Decarboxylation
Sustainable fuels
Kinetic model

ABSTRACT

Reaction kinetic studies were carried out of the reversible interconversion between γ-valerolactone (GVL) and pentenoic acid (PEA) combined with the irreversible decarboxylation of both species to form butene and CO_2 over a SiO_2/Al_2O_3 catalyst at pressures from atmospheric to 36 bar, temperatures from 498 to 648 K, different concentrations of GVL and PEA, as well as in the presence of water. The catalyst exhibited reversible deactivation within the initial 24 h on stream (losing about 50% of the initial catalytic activity), followed by a slower rate of deactivation of roughly 0.4–0.5% per hour on stream. Decarboxylation of γ-valerolactone, producing equimolar quantities of butene and CO_2, may possibly occur by two distinct pathways: a direct route from the lactone and an indirect route from PEA. 1-butene is the primary product of decarboxylation, formed via β-scission of intermediate carbenium ions. The apparent activation barrier for decarboxylation of GVL (175 kJ mol^{-1}) is higher than for decarboxylation of PEA (142 kJ mol^{-1}). A simple kinetic model with rate expressions accounting for adsorption and unimolecular surface reactions of GVL and PEA is sufficient to describe the trends measured for the rates of GVL ring opening to PEA, GVL decarboxylation, PEA cyclization to GVL, and PEA decarboxylation at different reaction conditions.

1. Introduction

Lignocellulose—the most abundant and inexpensive form of biomass—has been identified as an attractive, renewable feedstock that, worldwide, offers the energy content of 30–160 billion barrels of oil equivalent (bboe) per year, estimates which exceed the current global rate of consumption [1]. A commonly employed strategy for the conversion of lignocellulosic biomass to transportation fuels begins with controlled decrease in the oxygen content to yield intermediate platform chemicals that retain sufficient functionality such that they can be coupled to yield larger hydrocarbons [2]. In this respect, several processes have been reported based on the formation of levulinic acid and its derivative γ-valerolactone, GVL [3–5], leading to the production of methyltetrahydrofuran [4], levulinate esters [6,7], valeric esters [8], gasoline [9], jet fuel [10], and diesel [11]. In the present study, we explore the reaction kinetics for the conversion of GVL to pentenoic acid (PEA) and equimolar quantities of butene and CO_2 over a silica/alumina catalyst; these steps being key components for a recently reported strategy for the conversion of GVL to liquid alkenes with molecular weights appropriate for gasoline and/or jet fuel [10].

In prior publications [10,12], we suggest that the ring opening of GVL to PEA is a reversible reaction over silica/alumina through a wide range of reaction conditions, i.e., at pressures from 1 to 35 bars and temperatures from 523 to 648 K. We also consider the possibility that decarboxylation may occur either directly from GVL or indirectly from PEA produced by ring opening of GVL, and both of these pathways should be irreversible under typical reaction conditions (in view of the favorable thermodynamics for the formation of CO_2). The overall reaction scheme can thus be written as illustrated in Fig. 1.

To explore the significance of each pathway in Fig. 1, we have collected reaction kinetics data for different partial pressures of GVL and PEA at various temperatures. In addition, we have studied the effect of water on the reaction kinetics for the conversion of GVL and PEA. Water is typically present in biomass-derived sources of GVL, and addition of water to GVL has been shown previously to be advantageous for achieving stable catalytic activity versus time-on-stream [10]. Further, to aid in the development of a representative kinetic model, we have attempted to quantify the extent to which direct GVL decarboxylation may contribute to the net rate of butene production via the analysis of reaction kinetics at short space times. Finally, we have developed a simple

Abbreviations: GVL, γ-valerolactone; PEA, pentenoic acid.

* Corresponding author.
E-mail address: dumesic@engr.wisc.edu (J.A. Dumesic).

0021-9517/$ - see front matter © 2011 Elsevier Inc. All rights reserved.
doi:10.1016/j.jcat.2011.05.011

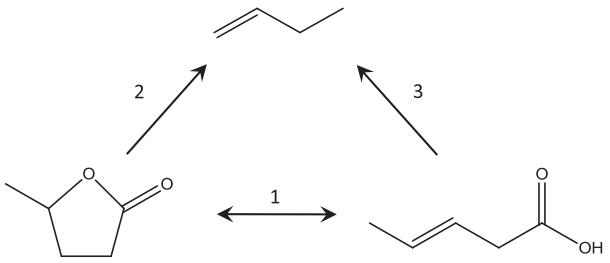

Fig. 1. Pathways for the production of butene from GVL and PEA over acid catalysts.

kinetic model, accounting for adsorption and unimolecular surface reactions of GVL and PEA on silica/alumina, to describe experimentally observed reactivity trends. We hope that insights gained from this study will guide the development of new catalysts and optimal processing strategies for the production of cellulosic biofuels.

2. Materials and methods

Amorphous SiO_2/Al_2O_3 (Grace Davison SIAL 3113) was calcined *in situ* in a fixed bed reactor at 723 K (heating rate of 3 K min^{-1}, followed by 4-h hold) in flowing air (Airgas, Medical Grade 50 cm^3(STP) min^{-1}) supplied by mass flow controller (Brooks Instruments, 5850S). Following calcination, the reactor was cooled to the reaction temperature under flowing air and then purged with flowing helium (Airgas, 20 cm^3(STP) min^{-1}) as the desired operating conditions were achieved. Periodic regeneration of SiO_2/Al_2O_3 was achieved using an identical protocol. γ-valerolactone (Sigma Aldrich, >98%), trans-2-pentenoic acid (Sigma Aldrich, 98%), and ethanol (Sigma Aldrich, 99.5%) were used without further purification. The surface area and mean pore diameter for the catalyst were estimated through nitrogen adsorption to be 450 m^2 g^{-1} and 4.5 nm, respectively. The alumina content of the material is 14 wt.%, as provided by the manufacturer.

2.1. Reaction kinetics studies

The ring opening of GVL, cyclization of PEA, and the decarboxylation of both reagents were studied in a fixed bed catalytic reactor operating in an up-flow configuration with pressures varied from atmospheric to 36 bar and temperatures from 548 to 648 K. The catalyst (SiO_2/Al_2O_3) was physically mixed with crushed quartz granules to maintain a consistent bed length for different experiments. The mixture was loaded into a stainless steel tubular reactor (6.35 mm OD) and held between two end plugs of quartz granules and quartz wool. Typically, GVL was introduced into the reactor in an aqueous solution (10–60 wt.% GVL), using an HPLC pump (Lab Alliance Series I). PEA is sparingly soluble in water (~2 wt.%) and was thus introduced using a high-pressure syringe pump (Harvard Apparatus, PHD 2000) along with a cofeed of water from an HPLC pump. The cofeed setup was also used in experiments designed to test the effect of GVL concentration. Helium was used to pressurize the reactor and separator at the reactor effluent, and air was introduced as necessary for periodic catalyst regeneration. Gas feed rates were controlled by mass flow controller (Brooks Instruments, 5850S). The tubular reactor was fitted inside an aluminum cylinder and placed within a well-insulated furnace (Applied Test Systems). Bed temperature was monitored at the reactor wall, using a Type K thermocouple (Omega) and controlled using a 16A series programmable temperature controller (Love Controls). Reactor pressure was controlled using a back pressure regulator (GO BP-60). The reactor effluent was diverted to a vapor–liquid separator, wherein the liquid product was collected. For the quantification of gas-phase species, the separator volume was purged by bubbling a helium sweep gas (10–50 cm^3 (STP)min^{-1}) through the liquid product.

Gas-phase products were analyzed using an in-line pair of gas chromatographs. A GC-2014 (Shimadzu) equipped with an FID detector was used for the analysis of hydrocarbon products, while CO and CO_2 were quantified using a GC-8A (Shimadzu) with a TCD detector using helium as a carrier/reference. Liquid samples were drained from the separator, and organic species were identified by GC-MS (Shimadzu GCQP-2010). To ensure accurate quantification of aqueous and organic product portions, the liquid product—commonly an emulsion of PEA, GVL, and water—was dissolved in ethanol and analyzed by HPLC, using an RI detector (Waters).

Individual experiments were designed such that contributions to the rate of key species (GVL, PEA, water) could be isolated. To this end, studies were carried out, wherein feed concentration, feed flow rate, and system pressure were modulated such that all reaction parameters other than the partial pressures of interest were held constant. Reaction conditions (catalyst loading, weight hourly space velocity (WHSV), and temperature) were selected such that total conversion of the feed molecule was maintained below 20%. To decouple the effects of interconversion between GVL and PEA, reactor feeds in this study were comprised of GVL or PEA in isolation rather than mixtures of the two. In this manner, we have quantified adsorption thermodynamics for each species separately prior to generalizing these results in a model that accounts for the adsorption of both species. Importantly, as GVL and PEA interconversion takes place at longer space times, we have observed that this model is effective in describing reactivity trends under conditions where both GVL and PEA are present in significant quantities. Thus, this treatment, although derived using single-reagent feed solutions, is appropriate for capturing reactivity trends under conditions where competitive adsorption of each species is significant.

Rates of GVL ring opening and PEA ring closure were, respectively, given by the observed production rates of PEA and GVL, with concentrations measured by HPLC. The rate of decarboxylation reported for various experiments is given as the average production rate of butene and CO_2. Butene and CO_2 concentrations were independently measured by GC-FID and GC-TCD. In all instances of decarboxylation, the molar ratio of butene to CO_2 was measured (within experimental error) to be 1.0, in accord with the mechanism proposed herein. Generally, total carbon balances closed to within 5%.

During our reaction kinetics studies, we observed that the SiO_2/Al_2O_3 catalyst undergoes slow deactivation at reaction conditions typical of GVL decarboxylation, after an initial period of more rapid deactivation (section 3.1). Additionally, we observed that the initial levels of activity could be restored completely by calcination of SiO_2/Al_2O_3 in air at 723 K. This behavior suggests that a practical mode of operation of the SiO_2/Al_2O_3 catalyst is to employ infrequent regeneration periods between lengthy periods of time-on-stream. Accordingly, the most relevant operating environment is that of a partially deactivated catalyst, and models were thus constructed to capture fundamental kinetics on this form of the catalyst. Thus, reaction kinetics experiments were standardized to a common state of deactivation by collecting data after an initial 72-h period of time-on-stream at a baseline condition. After this period of time, the loss of activity stabilizes to a rate that does not significantly alter trends (0.4% loss in activity per hour). Each set of experimental data was then collected within a period of 24 h, typically within 10 h. The maximal loss of catalytic activity is predicted to be roughly 10% over 24 h for a feed containing 60 wt.% GVL at 623 K. With the exception of data points at high oxygenate partial pressures (Sections 3.4.1 and 3.4.2), reaction kinetics studies were carried out using more dilute feeds, leading

to a slower rate of deactivation. In addition, for each experimental data set, reaction conditions were varied in a random fashion to avoid superposition of catalyst deactivation onto trends in reaction kinetics data. In representative experiments, data were first collected at baseline reaction conditions; data were then collected by randomly varying a specific variable (e.g., temperature, partial pressure); the data set was completed by returning to the baseline reaction conditions and measuring catalytic activity. By this method, we verified that significant deactivation (>5%) does not take place over the course of a single data set, which is consistent with the rate of deactivation reported in Section 3.1. In modeling trends in reactivity, initial rate data were estimated at a common time-on-stream, using the deactivation constant reported herein.

To ensure that the reactions described herein are catalytic, we have examined the extent of interconversion and decarboxylation of both GVL and PEA in the absence of catalyst (SiO_2/Al_2O_3). No decarboxylation products are observed from either GVL or PEA at the highest temperature reported in this study (648 K). Similarly, the interconversion between GVL and PEA does not occur at temperatures at or below 648 K. The onset of decarboxylation from GVL begins, in the absence of a solid acid catalyst, at roughly 873 K. Thus, the reactions considered here occur catalytically over SiO_2/Al_2O_3.

In this study, we have addressed the possible influence of both intraparticle and external transport limitations on controlling observed rates of reaction. Regarding external mass transfer limitations, we consider the relationship given by Eq. (1), which indicates that external transport limitations are not governing provided that the dimensionless group on the left-hand side of the inequality is less than 0.15 for a first-order reaction [13]. In this expression, *Rate* is the total rate of reaction (ring opening/ring closure plus decarboxylation) per unit volume of catalyst, R_p is the radius of a representative particle of SiO_2/Al_2O_3, C_b is the bulk concentration of GVL or PEA in the reactor feed, k_c is the mass transfer coefficient between the catalyst and bulk phases, and n is the reaction order (taken to be 1 for this system).

$$\frac{Rate \cdot R_p}{C_b \cdot k_c} < \frac{0.15}{n} \tag{1}$$

Reaction rates and bulk oxygenate concentrations were taken from representative reaction kinetics measurements reported in this work. The particle radius was estimated using a graduated series of standard mesh screens (40–230). The powdered SiO_2/Al_2O_3 used in this study was observed to pass through a 230 mesh screen, indicating a maximum particle diameter of 0.063 mm. Mass transfer coefficients were obtained using standard correlations for gas flow through packed beds [14]. At the conditions of this study, the dimensionless group was generally estimated to be on the order of 0.001. For 4 of the 79 data points considered, experimental conditions were particularly demanding, leading to an elevated rate of reaction at a temperature of 648 K and a low oxygenate partial pressure of roughly 0.02 bar. In this case, we estimate that the dimensionless group increases by an order of magnitude to 0.01. Importantly, the value in this limiting case remains below the threshold suggested in Eq. (1). As such, we do not consider interphase transport to limit the rate of reaction at the conditions reported herein.

To probe the extent of transport control within catalyst particles, we have estimated the Weisz–Prater number as given by Eq. (2) [15]:

$$N_{W-P} = \frac{Rate \cdot R_p^2}{C_s D_{eff}} \tag{2}$$

Rate and R_p are defined as in the preceding paragraph, and C_s is the reactant concentration at the catalyst surface. In the absence of external transport limitations, we consider C_s to be equal to the bulk oxygenate concentration. D_{eff} is estimated by Eq. (3) as the product of the porosity (p) and the Knudsen diffusivity (D_{Kn}).

$$D_{eff} = p \cdot D_{Kn} \tag{3}$$

The porosity was taken to be 0.5 for SiO_2/Al_2O_3, and the Knudsen diffusivity was estimated as per Vannice [15]. According to the Weisz–Prater criteria, rate control by intraparticle transport becomes significant at values of N_{W-P} greater than 0.3. We have observed that, at temperatures below 600 K, the values of the Weisz–Prater number were typically on the order of 0.005 and clearly in the kinetically controlled regime. The value of N_{W-P} increases to 0.08 at the highest temperature considered in this study (648 K), suggesting that intraparticle diffusion is not rate limiting, even under the most demanding conditions tested.

As a final consideration, we observe that the apparent activation energy in Arrhenius plots (Section 3.3) is constant as experimental conditions transition from low to high temperatures. The clearly demonstrated absence of transport limitations at the lower temperatures combined with a constant apparent activation barrier over the entire range of temperatures indicates that the experimental data are kinetically controlled and free from both internal and external transport limitations throughout this study.

2.2. Reaction model development

Linearized models of experimental data were used to describe observed trends, for instance in Arrhenius plots to estimate apparent activation energies. Estimation of the slope was achieved using linear least squares, and confidence intervals on estimates were calculated at 95% confidence. Kinetic models were developed according to observations from studies designed to elucidate the effects of temperature and concentrations of relevant species, and parameters were assessed for sensitivity by measuring the change in predicted rates of reaction produced for a 10% perturbation in initial parameter values. Insensitive parameters were lumped where possible to reduce the total number of variable parameters. Robust nonlinear least squares analysis was carried out using MATLAB (nlinfit) and resulted in optimized parameter estimates and ranges of confidence intervals. The inclusion of a parameter governing a direct pathway for GVL decarboxylation is considered according to the Akaike Information Criteria, as presented in Section 3.5.

3. Results and discussion

3.1. Catalyst stability versus time-on-stream

Fig. 2 shows a plot of catalytic activity for GVL conversion to butene as a function of time-on-stream. The data presented show the natural logarithm of the rate of decarboxylation (r) normalized by the initial rate of decarboxylation (r_0), which was obtained by linear extrapolation of the trend observed in the initial data points to zero time-on-stream. In Fig. 2, we observe that the rate decreases by about 50% within the initial 24 h on stream. Afterward, the system stabilizes and a lower rate of deactivation is observed, with the activity decreasing by roughly 0.4–0.5% per hour on stream. Accordingly, experiments designed to elucidate the effects of temperature and changes in the concentrations of GVL, PEA, and water were carried out after the system reached conditions at which the rate of deactivation did not significantly affect trends in data. Because the initial activity of the catalyst can be regenerated by calcination, catalyst deactivation is likely caused by deposition of coke. To test this hypothesis, we have carried out temperature-programmed oxida-

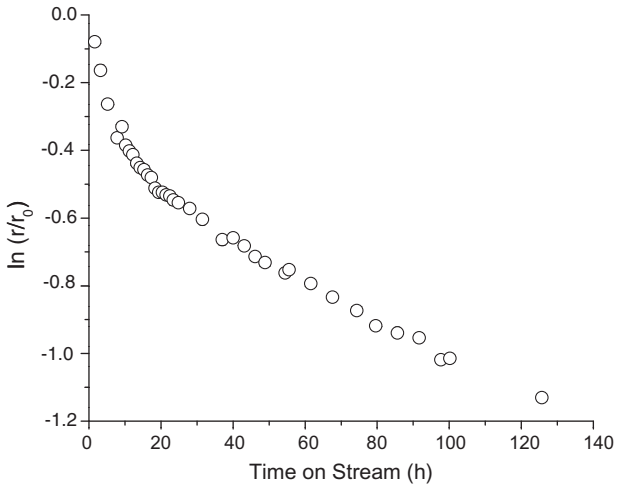

Fig. 2. Rate of butene production from GVL as a function of time on stream. WHSV = 3.7 h^{-1}, P = 1 bar, T = 623 K.

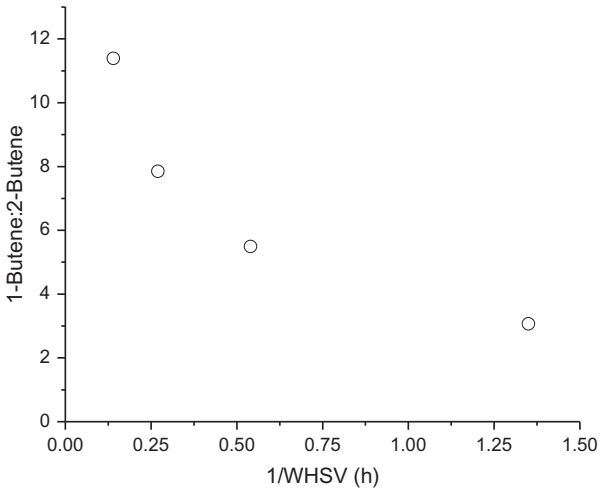

Fig. 3. Molar ratio of butene isomers as a function of GVL WHSV at 613 K and 1 bar using a feed of 60 wt.% GVL in water.

tion of catalysts that have been exposed to baseline reaction conditions for a period of 72 h on stream. Indeed, these TPO studies show the formation of CO and CO_2 upon the oxidation of spent SiO_2/Al_2O_3, leading to complete restoration of initial catalytic activity. We suggest that coke formation arises from polymerization of either GVL or PEA, which are demonstrated to interact strongly with SiO_2/Al_2O_3, rather than by polymerization of the butene product. We did not observe expected products of butene oligomerization (e.g., octene, and dodecene) or cracking (e.g., ethylene, and propylene), and the extent of butene isomerization at the elevated space velocities studied is minimal. Rather, we observed equimolar quantities of butene and CO_2 in the reactor effluent. These observations suggest minimal interaction of butene with the catalyst surface in the presence of feed oxygenates and water. We have previously observed severe competitive inhibition by water in butene oligomerization over solid acids [10], supporting a preferential coordination of water and a minimal involvement of the butene product in catalyst deactivation.

3.2. Reaction pathways

Variation in the space time has a pronounced effect on the distribution of butene isomers measured in the reactor effluent, suggesting that butene isomerization is not sufficiently rapid to become equilibrated. The trend in the observed ratio of 1-butene:2-butene as a function of space time (1/WHSV) is presented in Fig. 3. We observe that 1-butene is the dominant product at 613 K, and the molar ratio 1-butene:2-butene present in the reactor effluent increases as the reactor space time decreases (higher WHSV), a result which can be attributed to a decrease in the extent of butene isomerization at short residence times. For comparison, prior studies indicate that the molar ratio 1-butene:2-butene at equilibrium is expected to be approximately 0.2–0.3 in the range of 604–623 K [16,17]. These results support the previously suggested pathway [12], whereby decarboxylation is proposed to occur preferentially through intermediates bearing carbenium ions β to the acid group, and C—C bond cleavage occurs between the α- and carbonyl carbons to produce 1-butene and CO_2, as shown

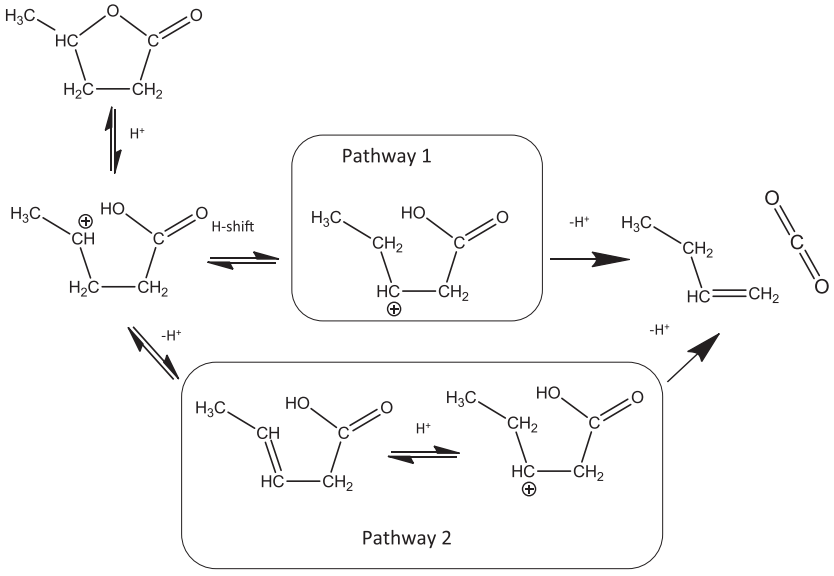

Fig. 4. Proposed mechanism of decarboxylation through an intermediate bearing a carbenium ion at the beta carbon.

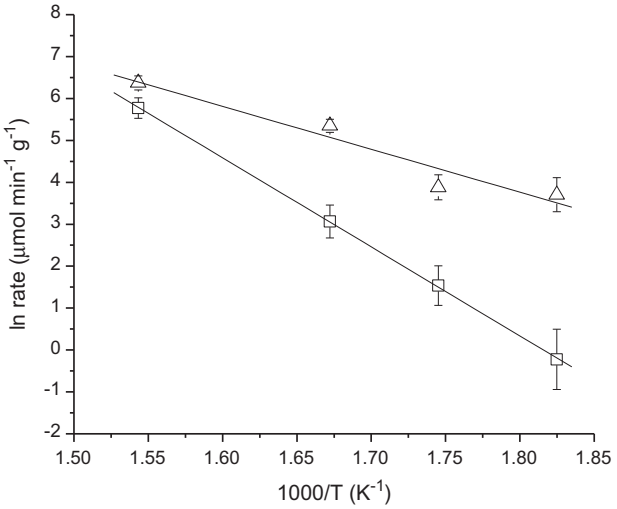

Fig. 5. Rates of reaction for ring opening (Δ) and decarboxylation (□) of γ-valerolactone at various reaction temperatures; feed is 10 wt.% GVL in water, WHSV = 15 h^{-1}, P = 1 bar.

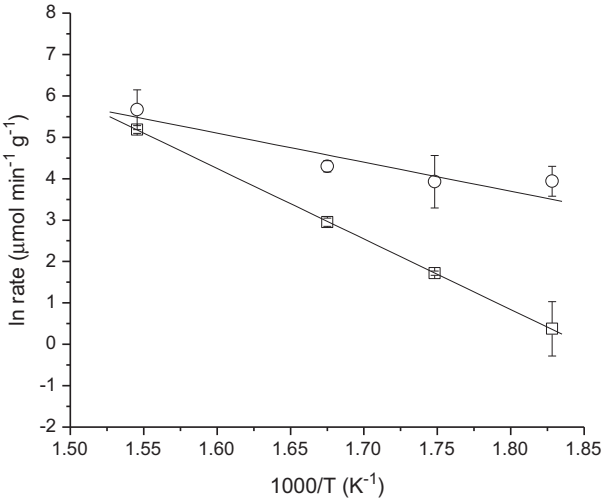

Fig. 6. Rates of reaction for ring closure (○) and decarboxylation (□) of trans-2-PEA at various reaction temperatures; feed is 10 wt.% trans-2-pentenoic acid in water, WHSV = 15 h^{-1}, and P = 1 bar.

in Fig. 4. This pathway is consistent with that suggested by Noyce et al. [18], who similarly proposed an initial activation of the β-carbon of β-phenylcinnamic acid via hydration in aqueous sulfuric acid, followed by dehydration/β-scission to yield diphenylethylene, water, and CO_2. In a related study [19], the authors observed similar selectivity toward decarboxylation products from β-lactones, supporting selective cleavage of the bond between the carboxyl group and the α-carbon over other possible β-scission pathways. In contrast to these prior reports, we suggest that a hydrated intermediate (hydroxy-pentanoic acid in this case) is not required because we have observed decarboxylation of GVL over SiO_2/Al_2O_3 in the absence of water. Additionally, under the conditions studied, we have not observed hydroxy-pentanoic acid by GC-MS analysis, suggesting that hydration is unfavorable at the temperatures reported over SiO_2/Al_2O_3. Subsequent to decarboxylation, isomerization of 1-butene occurs over acidic sites to yield cis-2 and trans-2 butene, which are the predominate products under conditions of high butene yield [10].

3.3. Effects of temperature

As indicated in Fig. 1, the net rate of butene production from GVL is potentially dependent on the reversible ring opening of GVL, combined with both direct and indirect decarboxylation pathways – of GVL and PEA respectively – both of which are irreversible. In a prior study [12], we have described the underlying thermodynamics of GVL ring opening to show that higher concentrations of PEA are favored by equilibrium at higher reaction temperatures. Fig. 5 summarizes the observed effect of reaction temperature on the rate of GVL ring opening and on the overall rate of decarboxylation. From this figure, we estimate that the apparent activation energies for ring opening and decarboxylation are equal to 85 ± 19 kJ mol^{-1} and 175 ± 20 kJ mol^{-1}, respectively (95% confidence intervals), when the feed to the reactor is comprised of GVL and water.

Additional experiments, plotted in Fig. 6, were carried out at analogous conditions with a feed of trans-2-pentenoic acid and water to observe the temperature dependencies of cyclization (to form GVL) and decarboxylation of PEA, which we propose to be an intermediate in the decarboxylation of GVL. Similarly, we observe stronger temperature dependence in the rate of decarboxylation, and apparent activation energies for cyclization and decarboxylation are estimated to be 58 ± 24 kJ mol^{-1} and 142 ± 11 kJ mol^{-1}, respectively (95% confidence intervals).

Comparing the rates of reaction of both GVL and PEA, we see that the activation barriers to ring opening (of GVL) and ring closure (of PEA) are relatively small and comparable for each reaction. Thus, a rapid interconversion between GVL and PEA is expected under typical reaction conditions, achieving equilibrium ratios of GVL to PEA at longer space times, as reported previously [12]. We observe a difference of 33 kJ mol^{-1} in the apparent activation barriers for decarboxylation of GVL and PEA, suggesting that C—C bond cleavage occurs more readily from PEA than directly from GVL and that butene production occurs predominately through the PEA intermediate. It is possible, however, that a pathway for direct decarboxylation of GVL exists, especially at short space times for which the partial pressure of PEA is low, as will be explored later in this paper.

3.4. Partial pressure dependencies

3.4.1. γ-valerolactone

Fig. 7 shows the results for the dependence of the rates of ring opening and decarboxylation on the partial pressure of GVL, from which we calculate apparent reaction orders of 0.16 ± 0.03 and 0.42 ± 0.09 for ring opening and decarboxylation of GVL, respectively. The observed trend in both ring opening and decarboxylation is an apparent fractional order dependence on GVL partial pressure, although a less pronounced dependence is observed in the rate of ring opening than that of decarboxylation. It is apparent that increases in GVL concentration yield only modest enhancements in rates of reaction, particularly in ring opening, and this behavior could potentially be attributed to a strong interaction between GVL and the surface of SiO_2/Al_2O_3, which causes saturation of acid sites and a diminished response to GVL partial pressure at high concentrations. The observation of different reaction orders with respect to ring opening and decarboxylation suggests that GVL concentration contributes differently to each reaction. It is possible that the higher reaction order observed in the rate of decarboxylation is indicative of the fact that, even at low extents of reaction, decarboxylation is primarily achieved through intermediate PEA rather than by direct decarboxylation of GVL.

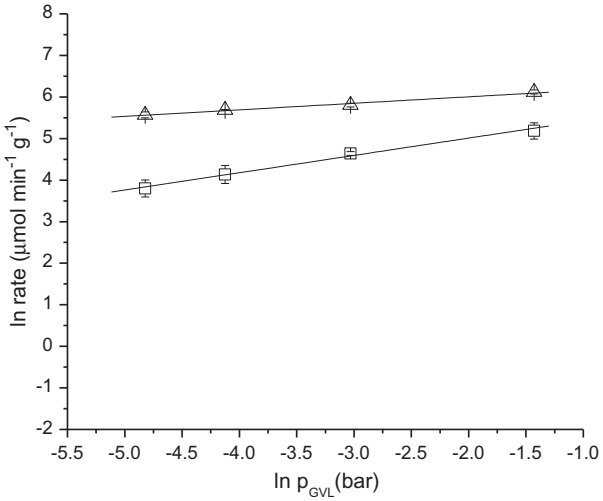

Fig. 7. Rates of reaction for ring opening (Δ) and decarboxylation (□) of γ-valerolactone at various partial pressures of GVL; T = 623 K, WHSV = 10 h^{-1}.

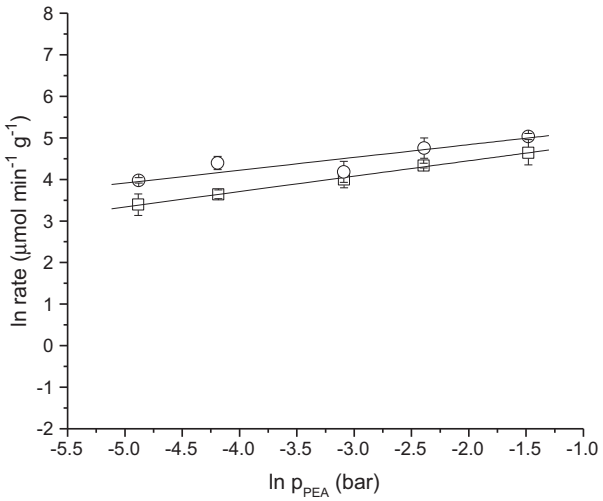

Fig. 8. Rates of reaction for ring closure (○) and decarboxylation (□) of trans-2-pentenoic acid at various partial pressures of PEA; T = 623 K, WHSV = 10 h^{-1}.

3.4.2. Pentenoic acid

Similar to the trends reported earlier with respect to changes in the GVL partial pressure, we observe in Fig. 8 a slightly positive reaction order in both the rate of ring closure (0.31 ± 0.07) and decarboxylation (0.37 ± 0.07) for the conversion of PEA over SiO_2/Al_2O_3. The observation of similar, fractional reaction orders for both ring closure and decarboxylation suggests that both reactions occur through a common coordination of PEA with the catalyst surface, which is likely indicative of a unimolecular surface reaction. PEA surface coverage has a strong effect on the overall rate of reaction, even at the low range of partial pressures described in this study, and its adsorption should be considered in governing rate expressions.

3.4.3. Water

We have observed previously that the presence of water is necessary to minimize the extent of catalytic deactivation in the production of butene [10]. Additionally, water is commonly considered to inhibit acid-catalyzed surface reactions by competing for adsorption at acid sites [20,21]. In Fig. 9, the rates of GVL ring opening and decarboxylation are plotted against the partial pressure of water on a logarithmic scale. In both cases, we observe that the rate of reaction has a negative, fractional reaction order with respect to water, equal to −0.65 ± 0.2 and −0.85 ± 0.45 for ring opening and decarboxylation of GVL, respectively, which is consistent with competitive surface coordination of water molecules.

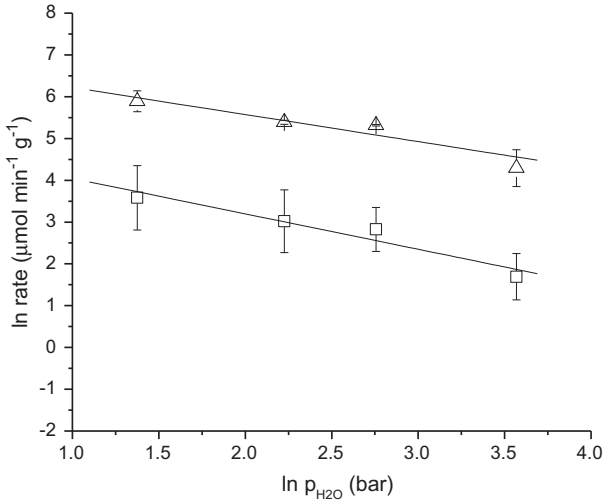

Fig. 9. Rates of reaction for ring opening (Δ) and decarboxylation (□) of GVL at various partial pressures of water; T = 623 K, WHSV = 10 h^{-1}.

3.5. Decarboxylation pathways

In Fig. 4, we outline two possible pathways by which decarboxylation of GVL may occur. Pathway 1 illustrates direct GVL decarboxylation, which takes place upon initial protonation to open the lactone ring followed by a proton shift to form a β-carbenium ion, which undergoes C–C cleavage to liberate 1-butene and CO_2. Pathway 2 suggests that decarboxylation may also occur, after ring opening, upon deprotonation (forming pentenoic acid) and reprotonation (forming a β-carbenium ion). In this section, we analyze the extent to which both pathways contribute to the net rate of butene production from GVL. It is important to note that contributions of either pathway may be influenced by the degree of deactivation in the acid catalyst. For example, freshly calcined catalysts having stronger acidity and a higher active site density may promote direct decarboxylation (pathway 1 of Fig. 4), whereas the dominant pathway may shift to indirect decarboxylation (pathway 2 of Fig. 4) as the catalyst deactivates and loses acidity. Here, we have elected to study the behavior of partially deactivated SiO_2/Al_2O_3, because this state will ultimately be more relevant to long-term industrial implementation.

The relative rates for the production of butene by direct decarboxylation of GVL or indirect decarboxylation of PEA can be probed by examining both the concentration of PEA and the net production rate of butene and CO_2 as functions of space time. Specifically, the rate of decarboxylation achieved in the limit of infinite space velocity (where GVL conversion and PEA concentration are expected to approach zero) allows quantification of the rate of decarboxylation in the absence of PEA. The results of this experiment are summarized in Fig. 10.

Fig. 10a illustrates the effect of space time on the effluent partial pressures of pentenoic acid, GVL, and butene (plotted on the right-hand axis) at 633 K using a 10 wt.% solution of GVL in water. Note that the partial pressure of the CO_2 coproduct was measured to be equal to that of butene and is not reported in a separate data set. We observe that the partial pressures of PEA and decarboxylation

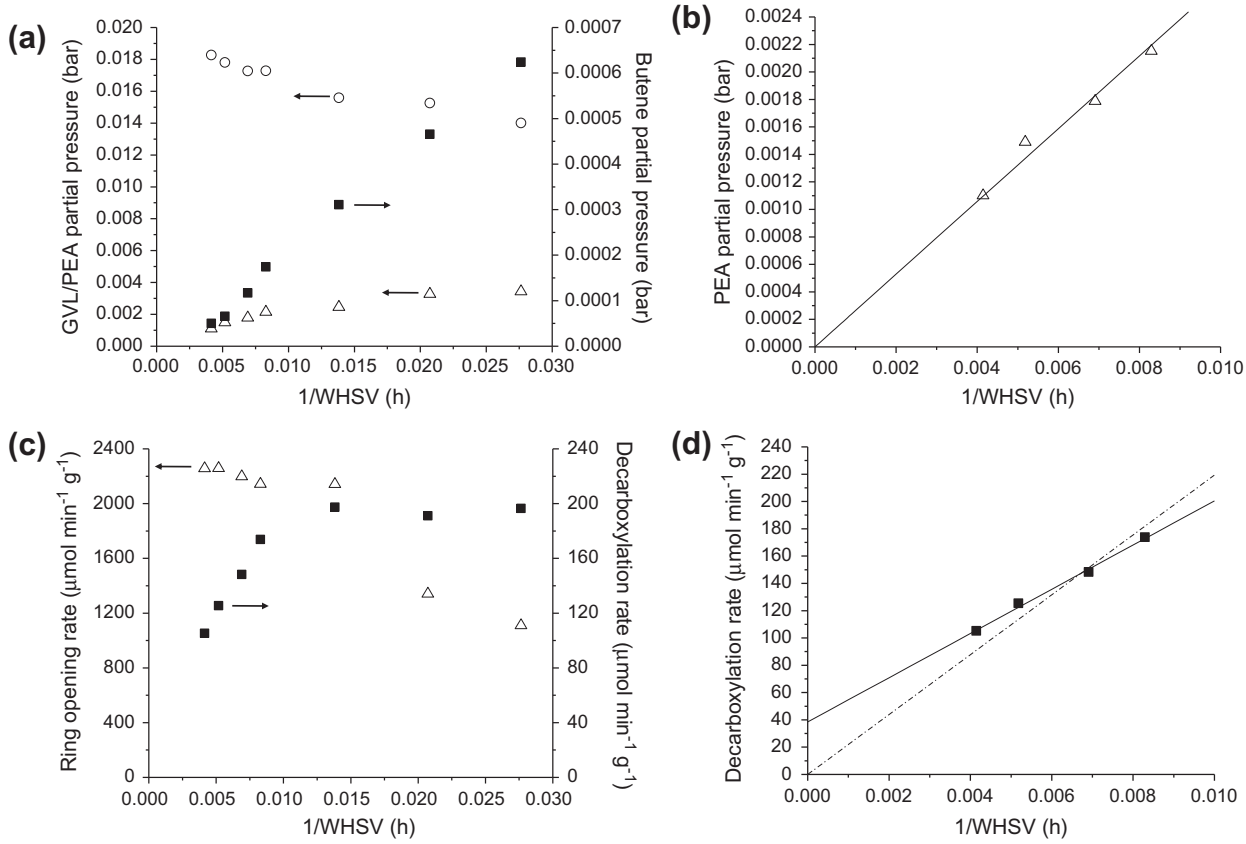

Fig. 10. Summary of reaction kinetics data obtained at short space times. (a) Outlet GVL (○), PEA (Δ), and butene (or CO_2) (■) partial pressures as a function of space time (1/WHSV). Butene (or CO_2) partial pressure (■) is plotted on the right-hand axis. (b) Extrapolation of PEA partial pressure (Δ) to the zero space time limit. (c) Rates of ring opening (Δ) and decarboxylation (■) as a function of space time (1/WHSV). The decarboxylation rate is plotted on the right-hand axis. (d) Extrapolation of the decarboxylation rate to the zero space time limit. The solid line represents a linear regression of the measured data while the dashed line is included to illustrate the requisite decarboxylation trend in the absence of a direct pathway for GVL decarboxylation. Experimental conditions for figures (a–d) 10 wt.% GVL in water, 633 K, WHSV of 36–240 h^{-1}.

products (butene and CO_2) decrease monotonically, ultimately approaching zero, with decreasing space time. The GVL partial pressure approaches that of the reactor feed (0.0198 bar) in the limit of zero space time. Fig. 10b provides an expansion of the trend in PEA partial pressure as space time approaches zero, and we observe a trend that is well described by a linear model with a zero *y*-intercept. The rate of ring opening in this limit is also shown (Fig. 10c). Taken together, these results suggest that PEA is a primary product of GVL conversion.

Fig. 10c shows rates of both ring opening and decarboxylation (plotted on the right-hand axis) as a function of space time. The rate of decarboxylation reported here quantifies the rate of either butene or (equivalently) CO_2 production, and we observe the two products in a 1:1 ratio under all conditions reported. The net rate of GVL ring opening decreases with increasing space time, which can be attributed to the onset of PEA ring closure and eventually GVL/PEA equilibration at relatively long space times. Fig. 10c also shows that the rate of decarboxylation remains constant at relatively long space times (0.015–0.030 h) and begins to decrease only at shorter space times (<0.01 h). The long space time limit is informative regarding the total rate of decarboxylation attainable at these conditions (~200 μmol min^{-1} g^{-1}). At shorter space times (<0.01 h), we observe a pronounced decrease in the partial pressure of PEA in the reactor effluent (Fig. 10a and b), which parallels a decrease in the overall rate of decarboxylation. This behavior suggests that at sufficiently short space times, the total production rate of butene is limited by the concentration of PEA; however, it is unclear whether PEA is a necessary precursor for decarboxylation. Fig. 10d provides an expansion of the trend in decarboxylation rate observed at short space times. In the limit of infinite space velocity, we observe by extrapolation that the rate of decarboxylation is predicted to be 38 ± 14 μmol min^{-1} g^{-1}, despite a clear indication that the partial pressure of PEA approaches zero under these conditions (Fig. 10b). The only species present in significant concentration at a space time of zero is GVL; therefore, the non-zero rate of decarboxylation can be attributed to a direct pathway for decarboxylation (pathway 1 of Fig. 4).

Given the proximity of the estimated y-intercept to zero, we acknowledge that such an extrapolation is tenuous evidence of a direct pathway for GVL decarboxylation. To facilitate a direct comparison of the implications of either outcome, we additionally illustrate in Fig. 10d the trend in decarboxylation predicted through a linear model with a y-intercept fixed at zero (dashed line). This model describes the necessary trend in the rate of butene production, as the partial pressure of PEA approaches zero, in the absence of a direct decarboxylation pathway. Although we cannot be absolutely confident in our estimate of the decarboxylation rate in the limiting case of infinite space velocity, the observed trend in Fig. 10d is better described by allowing a positive y-intercept corresponding to a non-zero rate of butene production in the absence of PEA.

To summarize, the experimental data at short space times suggest the possibility of direct GVL decarboxylation, and our subsequent models have thus considered both of the proposed decarboxylation pathways. Quantitatively, we estimate that direct GVL decarboxylation could contribute as much as 10–20%

(38 μmol min^{-1} g^{-1}) to the total rate of butene/CO_2 production (200 μmol min^{-1} g^{-1}).

3.6. Kinetic model

Over the range of partial pressures studied, we observe a positive, fractional order dependence with respect to the GVL and PEA concentrations on the rates of GVL ring opening and PEA cyclization, respectively. Thus, adsorption of both GVL and PEA appears to be favorable on the surface of SiO_2/Al_2O_3 and influences the rates of all important reactions. We have observed that decarboxylation of GVL proceeds with a higher apparent activation barrier than decarboxylation of PEA. As presented earlier, data collected at short space times suggest that consideration of both direct and indirect decarboxylation pathways may be necessary to accurately describe trends in reaction kinetics data. Indeed, we have observed enhanced predictive capabilities upon the inclusion of a direct pathway in governing kinetic models, as described in subsequent paragraphs. The rate of decarboxylation has a fractional order dependence with respect to the concentrations of both GVL and PEA, suggesting again that adsorption of these species is important in both pathways for decarboxylation. Finally, we have observed that water has an inhibiting effect on both ring opening and decarboxylation, which can be attributed to competitive binding at the active sites.

We assume that each of the three reactions in Fig. 1 can be considered a unimolecular surface reaction and that adsorption of water, PEA, GVL, and butene can contribute in each rate expression. In this study, experiments were typically carried out at elevated temperatures and low extents of reaction, which resulted in low partial pressures of butene in the reactor. Thus, adsorption of butene is not expected to compete with that of water, GVL, and PEA, all of which have demonstrated significant interactions with the catalyst surface. This assumption is supported by our observation of products rich in 1-butene under the conditions studied, suggesting that butene adsorption/isomerization is not occurring rapidly in the presence of other, strongly adsorbed species. Additionally, we have not observed butene oligomers or cracking products in the reactor effluent. Therefore, butene adsorption is not considered in the governing rate expressions. The rates of all relevant reactions can be expressed as a product of rate constants (k_i) and surface coverages (θ_i) for each species, as summarized in Eqs. (4)–(6). The surface coverage expressions are given by Eq. (7), the denominator of which includes coefficients and partial pressures dependencies for adsorption of water, GVL, and PEA. The effect of water has been isolated from that of GVL and PEA to decouple its influence and allow for more efficient capture of trends related to water partial pressure, and an exponent parameter (n, m) is included for each factor to assist in capturing disparate reaction orders observed experimentally in GVL, PEA, and water.

$$r_1 = k_1 \cdot \theta_{GVL} - k_{-1} \cdot \theta_{PEA} \tag{4}$$

$$r_2 = k_2 \cdot \theta_{GVL} \tag{5}$$

$$r_3 = k_3 \cdot \theta_{PEA} \tag{6}$$

$$\theta_i = \frac{K_i \cdot p_i}{(1 + K_{GVL} \cdot P_{GVL} + K_{PEA} \cdot P_{PEA})^m \cdot (1 + K_{H_2O} \cdot P_{H_2O})^n} \tag{7}$$

We note here that we do not have sufficient information (e.g., from density functional theory, microcalorimetry, *in situ* spectroscopy) to build a proper micro-kinetic model for this surface chemistry. Therefore, we have employed a rather semi-empirical model to capture the trends in the reaction kinetics. We have found that the use of two site-blocking terms in the denominator is necessary to describe the experimental data, suggesting that two different types of sites are involved in the chemistry (e.g., the combination of a Brønsted and a Lewis acid site). This observation could now serve as the impetus for theoretical calculations. Because we are using a semi-empirical model, we express the rate constants in expressions 4–6 simply, according to the compensation effect [22], as the product of a rate constant estimated at the average temperature of the study (595 K) and an activation energy as given in Eq. (8), a construct which is effective in decoupling temperature effects and aids in the estimation of activation barriers [23].

$$k_i = k_{o_i} \cdot e^{\left(\frac{-E_A}{R}\left(\frac{1}{T}-\frac{1}{T_o}\right)\right)} \tag{8}$$

Adsorption parameters (K_i) can be expressed in a similar manner as dependent on binding energies, presented in Eq. (9).

$$K_i = K_{o_i} \cdot e^{\left(\frac{-\Delta H_{ads}}{R}\left(\frac{1}{T}-\frac{1}{T_o}\right)\right)} \tag{9}$$

In Fig. 11, we demonstrate that the rate expressions given by Eqs. (4)–(9) are sufficient to capture the experimental observations, particularly those of butene production rates, which are the most significant in the interest of fuel production. Fig. 11a and b demonstrate good predictions by the model (in both GVL/PEA interconversion and decarboxylation) of the trends observed with varied partial pressures of both GVL and PEA. In addition, the model adequately describes the inhibitive effect of water on both GVL ring opening and decarboxylation, as illustrated in Fig. 11c. The temperature dependencies for GVL ring opening/decarboxylation and PEA cyclization/decarboxylation are illustrated in Fig. 11d and e, respectively. Estimated activation barriers are generally sufficient to capture observed trends in the data.

Estimates for kinetic parameters described in Eqs. (4)–(9) are summarized in Table 1. In the range of experimental conditions studied, we found that the binding energies for adsorption described in Eq. (9) were relatively insensitive; as such, the temperature dependence was eliminated and each constant was treated as a lumped parameter, K_o, at the average temperature. The activation barriers for the rate constants were fixed to the apparent values obtained through the linear regression of temperature-dependent reaction rates in the Arrhenius plots (Section 3.3). This approximation was effective in capturing global trends in rate of reaction while allowing a reduction in the total number of variable parameters without decreasing the predictive capabilities of the model. The kinetic model derived from Eqs. (4)–(9) contains thirteen parameters, nine of which were varied in optimization studies to fit the data. The remaining four (activation barriers) were fixed at independently estimated values.

We have assessed the necessity of including both direct and indirect pathways (Fig. 4) through consideration of the Akaike information criterion (AIC_c), calculated as in Eqs. (10) and (11), where k represents the number of parameters, n is the number of experimental observations, and RSS is the residual sum of squares calculated for the optimal parameter set [24].

$$AIC = 2k + n \cdot \left[\ln\left(\frac{2\pi RSS}{n}\right) + 1\right] \tag{10}$$

$$AIC_c = AIC + \frac{2k(k+1)}{n-k-1} \tag{11}$$

The addition of a parameter is justified provided that any resultant decrease in residual error is sufficient to offset the positive contribution of an increased parameter number and yield an overall decrease in the value for AIC_c. Using a data set of 79 experimental points covering a range of temperatures and GVL and PEA partial pressures, the optimal 9-parameter set presented in Table 1 yields a residual square error of 3.10. In contrast, for an 8-parameter model (which did not include a direct pathway for GVL decarboxylation), the minimum residual achieved is 5.71. The corresponding AIC_c values are 34.7 and −11.1 for the 8- and 9-parameter models

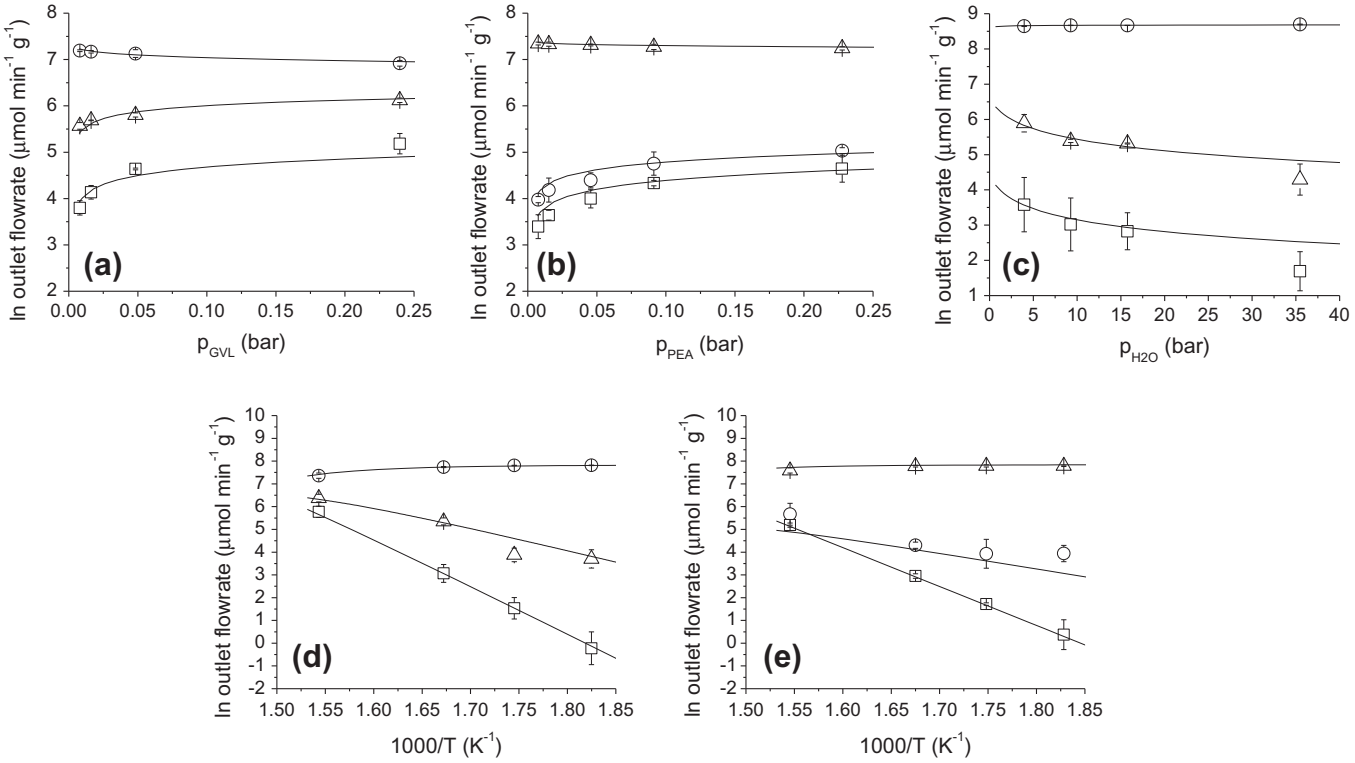

Fig. 11. Comparison between model predicted trends (solid lines) and experimentally observed molar flow rates of GVL (○), PEA (Δ), and butene(or CO_2) (□) in the effluent of plug flow reactors operating at various conditions. (a) Describes the trends observed in the effluent molar flow rates versus the GVL partial pressure. (b) Describes the trends observed in the effluent molar flow rates versus the PEA partial pressure. (c) Describes the trends observed in the effluent molar flow rates versus the water partial pressure. (d) Describes the trends observed in the rates of GVL ring opening and decarboxylation at various reaction temperatures. (e) Describes trends observed in the rates of PEA cyclization and decarboxylation at various reaction temperatures.

Table 1
Summary of kinetic parameters estimated by nonlinear least squares.

Parameter	Symbol	Optimized value	Physical contribution
1	K_{GVLo}	590 ± 13 bar^{-1}	Adsorption of GVL
2	K_{PAo}	1.4E + 03 ± 510 bar^{-1}	Adsorption of PEA
3	K_{H2Oo}	1.1 ± 0.022 bar^{-1}	Adsorption of water
4	E_{A1}	85[a] kJ mol^{-1}	Activation barrier of GVL ring opening
5	E_{A-1}	58[a] kJ mol^{-1}	Activation barrier of PEA cyclization
6	E_{A2}	175[a] kJ mol^{-1}	Activation barrier for direct GVL decarboxylation
7	E_{A3}	142[a] kJ mol^{-1}	Activation barrier for PEA decarboxylation
8	k_{1o}	0.27 ± 0.006 min^{-1}	Average rate constant for GVL ring opening
9	k_{-1o}	0.063 ± 0.013 min^{-1}	Average rate constant for PEA cyclization
10	k_{20}	0.024 ± 0.0006 min^{-1}	Average rate constant for GVL decarboxylation
11	k_{30}	0.017 ± 0.003 min^{-1}	Average rate constant for PEA decarboxylation
12	m	0.74 ± 0.003	Exponent for PEA and GVL adsorption
13	n	0.52 ± 0.010	Exponent for water adsorption

[a] Parameter value fixed.

respectively. Because the variation of a nineth parameter (specifically, one governing direct GVL decarboxylation) decreases the value of AIC_c, its inclusion is statistically justified. Qualitatively, we have observed that it is not possible to simultaneously capture trends in the rate of GVL ring opening and net decarboxylation without the consideration of a direct pathway.

In general, the parameter values obtained through least squares estimation agree with expectations from the qualitative analyses above. First, we observe that the adsorption coefficients (K_o) for GVL, PEA, and water are 590, 1400, and 1.1 respectively. These values suggest that the binding of both GVL and PEA is favorable on SiO_2/Al_2O_3, especially when compared to water. Assuming a common pre-exponential factor for adsorption and an average reaction temperature of 595 K, we estimate that a small difference in binding energy (<5 kJ mol^{-1}) can lead to the observed differences in K_o for GVL and PEA on SiO_2/Al_2O_3. The substantially smaller coefficient for water adsorption could be attributed to a binding energy that is weaker than that of GVL/PEA by roughly 35 kJ mol^{-1}. Typically, for experiments designed to assess reaction orders, the partial pressures of feed oxygenates were varied in the range of 0.01–0.2 bar, while the partial pressure of water was fixed at 1.5 bar, at which conditions we observe that oxygenate adsorption occurs sufficiently strongly such that adsorbed GVL and PEA account for significant portions of the total surface coverage.

By employing an estimate of 85 kJ mol^{-1} for the activation barrier of GVL ring opening, we adequately capture trends in experimental data. Similarly, an estimated barrier of 58 kJ mol^{-1} for ring closure of PEA is a reasonable approximation, which is

consistent with thermodynamic expectations that the conversion of GVL to PEA is an endothermic reaction. We consider this outcome in the context of Eq. (12), where the barrier to ring formation is expressed relative to that of ring opening, binding energies for GVL and PEA, and the enthalpy change between gas-phase GVL and PEA, suggested by prior studies to be endothermic and dependent upon the isomer of PEA considered. It has been demonstrated that the ring opening of GVL occurs with an enthalpy change of 17–40 kJ mol^{-1} in computational [12] and experimental studies [25]. We expect that for comparable binding energies of GVL and PEA (as suggested by the magnitude of adsorption coefficients), the forward barrier would exceed that of the reverse barrier for this endothermic reaction, and the model is thus consistent with the expected thermodynamics of GVL ring opening.

$$E_{A_{-1}} = E_{A_1} + \Delta H_{GVL_{ads}} - \Delta H_{PEA_{ads}} - \Delta H_{rxn} \quad (12)$$

Quantitatively, the difference in magnitude of forward and reverse activation barriers observed here (27 kJ mol^{-1}) is in the range suggested by previously reported reaction enthalpies. This result suggests that adsorptions of GVL and PEA occur with similar binding energies and supports observations that both species interact with the catalyst surface strongly and with comparable observed reaction orders.

Excellent agreement is achieved with respect to trends in butene production using activation barriers for decarboxylation of GVL and PEA of 175 and 142 kJ/mol, respectively, suggesting that butene production from PEA is the lower-energy pathway; however, at typical temperatures of decarboxylation and within the precision of the estimate, we cannot eliminate the possibility of direct GVL decarboxylation, especially at short space times. Values of k_o are taken to be representative of the rate constant for each reaction considered at the average temperature of the data set (595 K), and these values are estimated to be 0.274, 0.0631, 0.0241, and 0.0173 min^{-1} for GVL ring opening, PEA cyclization, GVL decarboxylation, and PEA decarboxylation, respectively. Thus, while the simple kinetic model outlined here is not intended as a definitive description of reactions occurring during the decarboxylation of GVL, this lumped model is effective in describing the rate of butene production under reaction conditions that would be expected in most biomass applications.

4. Conclusions

In a previous publication, we reported the production of butene from GVL followed by subsequent oligomerization to produce fuel-grade liquid alkenes [10]. In the present work, we report results for the reaction kinetics of the decarboxylation of GVL and PEA and their interconversion over a SiO_2/Al_2O_3 catalyst. In addition to the catalytic decarboxylation of PEA, we consider that direct decarboxylation of GVL may also contribute to the total rate of butene production (corresponding to about 10–20% of the overall rate at typical reaction conditions). The increasing ratio 1-butene:2-butenes in the product mixture with decreasing space time supports a mechanism where 1-butene is first formed via β-scission of intermediate carbenium ions. The simple kinetic model developed in this work provides a useful tool for predicting the rates of butene production for a wide range of reaction conditions. The results from this study can be used to aid in reactor design and process optimization studies to assess the techno-economic feasibility of producing liquid transportation fuels by the conversion of lignocellulosic biomass to GVL combined with catalytic decarboxylation to produce butene and alkene oligomers.

Acknowledgments

This work was supported by the Defense Advanced Research Projects Agency (DARPA) and Army Research Lab (ARL) through the Defense Science Office Cooperative Agreement W911NF-09-2-0010/09-005334 B 01 (Surf-Cat: Catalysts for production of JP-8 range molecules from lignocellulosic biomass). The views, opinions, and/or findings contained in this article are those of the authors and should not be interpreted as representing the official views or policies, either expressed or implied, of the Defense Advanced Research Projects Agency or the Department of Defense. In addition, this work was supported in part by the US Department of Energy Office of Basic Energy Sciences.

References

[1] G.W. Huber, B.E. Dale, Sci. Am. 301 (2009) 52.
[2] D. Martin Alonso, J.Q. Bond, J.A. Dumesic, Green Chem. 12 (2010) 1493.
[3] I.T. Horvath, H. Mehdi, V. Fabos, L. Boda, L.T. Mika, Green Chem. 10 (2008) 238.
[4] H. Mehdi, V. Fabos, R. Tuba, A. Bodor, L.T. Mika, I.T. Horvath, Top. Catal. 48 (2008) 49.
[5] H. Heeres, R. Handana, D. Chunai, C.B. Rasrendra, B. Girisuta, H.J. Heeres, Green Chem. 11 (2009) 1247.
[6] Texaco/NYSERDA/Biofine, Ethyl levulinate D-975 Diesel Additive Test Program, 2000.
[7] P.J. Fagan, L.E. Manzer, US Patent 7 153 996 to E.I. du Pont de Nemours and Company, 2006.
[8] J.P. Lange, R. Price, P. Ayoub, J. Louis, L. Petrus, L. Clarke, H. Gosselink, Angew. Chem. Int. Edit. 49 (2010) 4479.
[9] J.C. Serrano-Ruiz, D.J. Braden, R.M. West, J.A. Dumesic, Appl. Catal. B-Environ. 100 (2010) 184.
[10] J.Q. Bond, D.M. Alonso, D. Wang, R.M. West, J.A. Dumesic, Science 327 (2010) 1110.
[11] D. Martin Alonso, J.Q. Bond, J.C. Serrano-Ruiz, J.A. Dumesic, Green Chem. 12 (2010) 992.
[12] J.Q. Bond, D. Martin Alonso, R.M. West, J.A. Dumesic, Langmuir (2010), doi:10.1021/la101424a.
[13] J.A. Dumesic, D.F. Rudd, L.M. Aparicio, J.E. Rekoske, A.A. Trevino, *The Microkinetics of Heterogeneous Catalysis*, American Chemical Society, Washington, DC, 1993.
[14] W.L. McCabe, J.C. Smith, P. Harriott, Unit Operations of Chemical Engineering, McGraw Hill, Boston, 2001.
[15] M.A. Vannice, Kinetics of Catalytic Reactions, Springer, New York, 2005.
[16] H.H. Voge, N.C. May, J. Am. Chem. Soc. 68 (1946) 550.
[17] D.M. Golden, K.W. Egger, S.W. Benson, J. Am. Chem. Soc. 86 (1964) 5416.
[18] D.S. Noyce, S.K. Brauman, F.B. Kirby, J. Am. Chem. Soc. 87 (1965) 4335.
[19] D.S. Noyce, E.H. Banitt, J. Org. Chem. 31 (1966) 4043.
[20] L. Smith, A.K. Cheetham, R.E. Morris, L. Marchese, J.M. Thomas, P.A. Wright, J. Chen, Science 271 (1996) 799.
[21] T. Okuhara, Chem. Rev. 102 (2002) 3641.
[22] M. Boudart, Kinetics of Chemical Processes, Prentice-Hall, Inc., Englewood Cliffs, NJ, 1968.
[23] T. Bligaard, K. Honkala, A. Logadottir, J.K. Nørskov, S. Dahl, C.J.H. Jacobsen, J. Phys. Chem. B 107 (2003) 9325.
[24] R.M. West, D.J. Braden, J.A. Dumesic, J. Catal. 262 (2009) 134.
[25] V.N. Emel'yanenko, S.P. Verevkin, E.N. Burakova, G.N. Roganov, M.K. Georgieva, Russ. J. Phys. Chem. A 82 (2008) 1521.